Ultraviolet camera measurements of passive and explosive (strombolian) sulphur dioxide emissions at Yasur volcano, Vanuatu

Ilanko, T.[1], Pering, T.D.[1*] Wilkes, T.C[1]., Woitischek, J.[2,3], D'Aleo, R.[4], Aiuppa, A[5]., McGonigle, A.J.S[1,6,7]., Edmonds, M[2]., Garaebaeti, E.[8]

[1] Department of Geography, University of Sheffield, Winter Street S10 2TN, UK
[2] Department of Earth Sciences, University of Cambridge, Downing Street CB2 3EN, UK
[3] BPI Institute, BP Institute, University of Cambridge, Madingley Rd, CB3 E0EZ, UK
[4] INGV, Sezione di Palermo, Via Ugo la Malfa 153, 90146, Palermo, Italy
[5] DiSTeM, Università di Palermo, Via Archirafi, 22, 90123 Palermo, Italy
[6] School of Geosciences, the University of Sydney, NSW2006, Australia
[7] Faculty of Health, Engineering and Sciences, University of Southern Queensland, Toowoomba, QLD 4350, Australia
[8] Geohazards Division, Vanuatu Meteorology and Geo-hazards Department, Lini Highway, Port Vila, Vanuatu

*Corresponding author: t.pering@sheffield.ac.uk

Abstract

Here, we present the first ultraviolet (UV) camera measurements of sulphur dioxide (SO_2) flux from Yasur volcano, Vanuatu, for the period 6th – 9th July 2018 and the first direct gas based measurements of explosive gas masses from this target. Yasur typically exhibits persistent passive gas release interspersed with frequent strombolian explosions. We used the 'PiCam' Raspberry Pi UV Camera system (Wilkes et al., 2017, 2016) engineered in a more compact format and powered through solar panels. Our daily median SO_2 fluxes range 4.0-5.1 kg s^{-1}, with maximum determined measurement uncertainty of -12.2% to +14.7%, including errors from: gas cell calibration drift, and associated with uncertainty in plume direction and distance, as well as plume velocity. This work highlights the use of particle image velocimetry for plume velocity determination, which was deemed to be more preferable than the typically used cross-correlation and optical flow methods, because of the ability to function over a range of plume conditions, leading overall to more reliable fluxes. We calculate SO_2 masses for strombolian explosions of 8 to 81 kg (mean of 32 kg), to our knowledge the first budget of explosive gas masses from this target, and through the use of a simple statistical measure using the moving minimum, which is novel in its application in this context, we estimate that passive degassing is the dominant mode of gas emission at Yasur, averaging 69% of the total gas released. Our work serves to further highlight the utility of UV camera measurements in volcanology and, in particular, the benefit of the multiple camera approach in error characterisation. This work also adds to our inventory of gas-based data to characterise the spectrum of strombolian activity across the globe, concerning Yasur which has received relatively little attention in terms of released gas fluxes, hitherto.

Highlights

- Long time series data collected using portable solar chargeable UV cameras.
- Particle image velocimetry (PIV) used for plume velocity measurements.
- SO_2 fluxes daily median values of 4.0-5.1 kg s^{-1}.
- SO_2 masses of strombolian explosions range 8 to 81 kg (mean 32 kg).

1. Introduction

Strombolian volcanism is one of the more common forms of basaltic explosive activity globally, associated with the rapid ejection of hot pyroclasts from a vent in a single impulsive burst (Blackburn et al., 1976; Taddeucci et al., 2015), with event frequencies ranging from seconds to minutes (Pering and McGonigle, 2018). Volcanoes with frequent strombolian activity include: the archetypal Stromboli, Italy (Patrick et al., 2007; Ripepe et al., 2002); Pacaya, Guatemala (Battaglia et al., 2018; Dalton et al., 2010); Erebus, Antarctica (Ilanko et al., 2015; Johnson and Aster, 2005; Oppenheimer et al., 2009; Sweeney et al., 2008); and the subject of this study Yasur, Vanuatu (Bani and Lardy, 2007; Kremers et al., 2013; Oppenheimer et al., 2006). Other volcanoes also known to produce strombolian activity include: Etna, Italy (Aiuppa et al., 2016; Branca and Del Carlo, 2005; Pering et al., 2015) Villarrica, Chile (Shinohara and Witter, 2005); Arenal, Costa Rica (Garcés et al., 1998; Szramek et al., 2006); Batu Tara, Indonesia (Gaudin et al., 2017a; Laiolo et al., 2018); and Shishaldin, USA (Vergniolle et al., 2004).

Classically, this style of behaviour has been related to the ascent from depth of elongated and over-pressured bubbles, which rapidly expand in length as they approach the surface, termed gas slugs (Taylor bubbles) (Del Bello et al., 2012; James et al., 2008; Seyfried and Freundt, 2000; Taddeucci et al., 2015). However, recent research has suggested that the causal driving mechanisms may be far more diverse (Barth et al., 2019; Suckale et al., 2016), and that the presence of crystal-rich layers in the magmatic column is important in the formation of strombolian explosions. To test these hypotheses, it is useful to investigate the manifested spectrum of strombolian activity at targets, including Yasur, where this behaviour is typical. In addition, recent studies have highlighted the importance of eruption frequency in determining the behaviour of ascending gas slugs (Gaudin et al., 2017a) as well as inter-slug interactions, leading to a classification of behaviour styles ranging from rapidly bursting slugs which may interact with one another during ascent, through to single bursting slugs, where interactions do not apply (Pering et al., 2017; Pering and McGonigle, 2018).

There are several instrumental means to obtain information about individual strombolian explosions, which are based on capture of: seismic (Chouet et al., 2003; Ripepe et al., 2002), infrasonic (Dalton et al., 2010; Delle Donne et al., 2016; Johnson and Ripepe, 2011; Marchetti et al., 2009), thermal (Patrick et al., 2007; Ripepe et al., 2002), and gas-derived (McGonigle et al., 2009; Pering et al., 2015; Pering et al., 2016; Tamburello et al., 2012) data. Here, we focus on gas emission rate measurements, using the ultraviolet (UV) camera, a frequently used technique for constraining gas release from persistently outgassing volcanoes (McGonigle et al., 2017; Pering et al., 2019a). The UV camera approach enables resolution of high-time

resolution fluctuations in the release of sulphur dioxide (SO_2) gas, and in tandem with a multi component gas analyser (Multi-GAS), which measures gas ratios when placed inside a volcanic plume (Aiuppa et al., 2005; Shinohara et al., 2015), it is possible to estimate the total gas emission rate (Pering et al., 2014). An important parameter in respect of generation mechanisms for strombolian explosions is the relative proportions of gas released during explosions to that released passively (Barth et al., 2019; Jaupart and Vergniolle, 1989, 1988; Parfitt, 2004; Suckale et al., 2016; Vergniolle and Jaupart, 1986). This 'active' to passive degassing ratio also provides information about conduit fluid dynamics (Gaudin et al., 2017a, 2017b; Pering et al., 2015; Pering et al., 2016). For example, Tamburello et al., (2012) discovered that the most efficient mode of degassing at Stromboli was actually the passive degassing, which contributed to ~77% of gas release, demonstrating the continued importance of passive gas release.

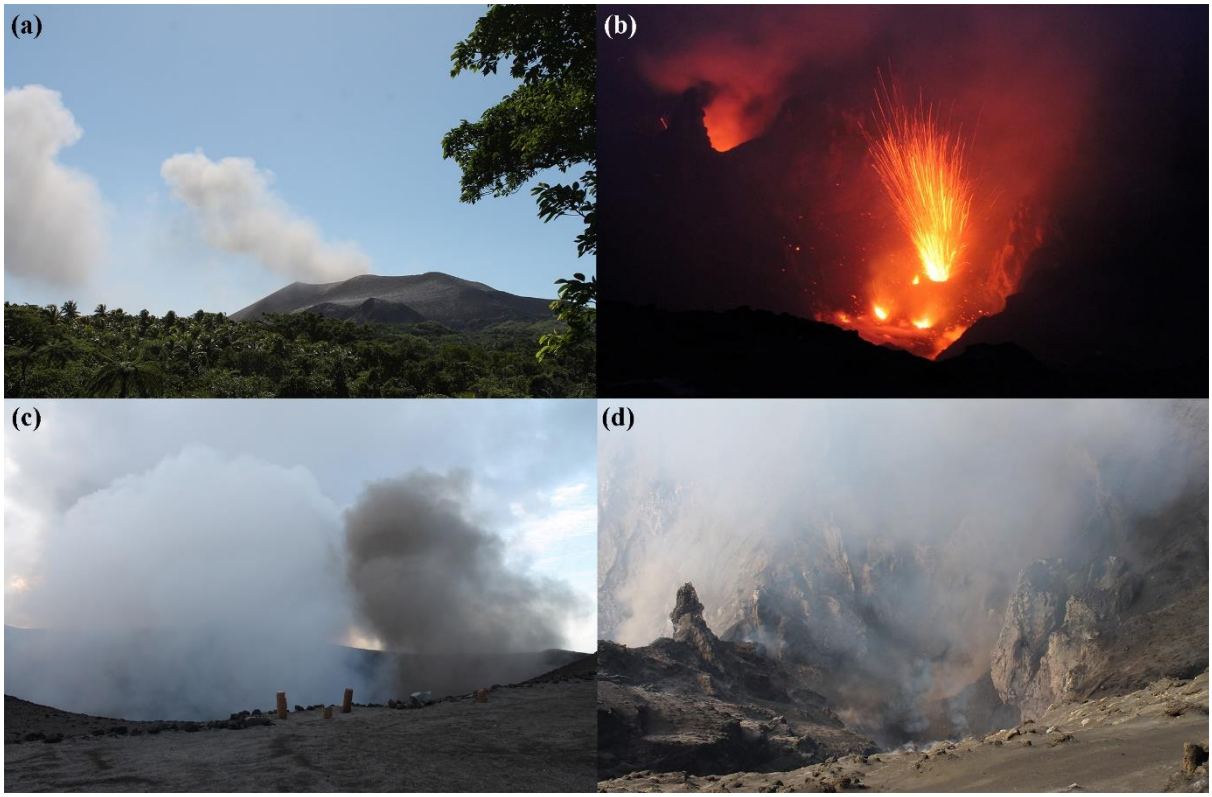

Figure 1: Example photos of activity during the field campaign. In (a) an image of the gas plume rising from the summit crater; large gas pulses are associated with explosions; (b) a night-time view with the south crater in the foreground and incandescence from the north crater in the background; several vents are visible in the south crater, as is a strombolian explosion, arising from one of them; (c) the gas rich plumes of the ash-rich strombolian explosions from the north crater contrasted against the ash-poor plume and explosions from the south crater; (d) a day-time view into the north crater, with the dividing inter-crater boundary on the image left-hand-side.

UV camera derived SO_2 masses from strombolian explosions (Mori and Burton, 2009; Pering et al., 2015; Tamburello et al., 2012) can also be combined with gas ratio data (e.g., from Multi-GAS), to generate total gas masses and volumes for individual explosive events (Burton et al.,

2007; Pering et al., 2016). These overall mass data can then be used to parameterise mathematical models for gas flow in conduits, to glean further information about the activity and generating mechanisms, for example, pertaining to slug length, explosive vigour, and categorisation of burst behaviour using fluid dynamics (Del Bello et al., 2012; James et al., 2009, 2008; Pering and McGonigle, 2018).

For this study we demonstrate the use of a very portable, solar-chargeable, version of the low-cost Raspberry Pi ultraviolet camera (Wilkes et al., 2017, 2016) combined with a new approach to plume velocity analysis for UV camera imagery to obtain sulphur dioxide fluxes. We present the first UV camera measurements at Yasur, providing the first gas-based estimate of explosive strombolian gas masses, key to unravelling information on the spectrum of behaviours on this style of activity globally. Furthermore, we illustrate the use of statistical methods to differentiate between passive and explosive gas release, and finally apply mathematical models to characterise the strombolian explosions at Yasur volcano.

2. Yasur volcano and activity during 5th-11th July 2018

Yasur (Vanuatu) is a basaltic stratovolcano located on the southeast of Tanna Island, which is thought to have been predominantly persistently active for at least ~800 years (Firth et al., 2014). The main volcanic edifice is a cone with a crater area of 350-450 m diameter, divided by a septum into northern and southern craters, each containing multiple active vents. During the field campaign measurement period an ashy plume was manifested throughout the week, related to ash-rich strombolian explosions arising from both craters (Fig 1). From the summit, multiple vents displaying incandescence were visible within the southern crater, each of which exhibited different styles of explosive behaviour. Gas release from the summit vents was constantly visible, occasionally including 'puffing' behaviour (Gaudin et al., 2017b, 2017a; Pering and McGonigle, 2018; Tamburello et al., 2012). The northern crater had at least two vents, but access to this crater's rim was prevented on the grounds of safety due to ballistic ejecta from the crater's strombolian explosions, which appeared to be more ash-rich than those from the southern crater. From the southern crater we directly observed explosions from at least three vents, each of which manifested different behaviours, two with jet-like characteristics (i.e., with a strong vertical component to the ejecta vector), highlighting the potential for interaction with the conduit wall during the explosion process, i.e., the explosion (slug burst) happens within the conduit, providing a vertical steer to the released material (Delle Donne and Ripepe, 2012). Another vent exhibited parabolic transport of incandescent pyroclasts, as though an ascending bubble burst within an over-topped magma column (Del Bello et al., 2012), or within a flared conduit geometry (Dibble et al., 2008). Interestingly these different styles of strombolian explosions also had clearly differentiable audible properties, with the latter associated with a deeper booming sound. During 8 – 9 July, explosions were frequently associated with visible shockwaves propagating through the condensed plume. The supplementary video highlights a snapshot of typical activity captured from the both craters. Throughout the measurement period, the morphology of the crater was dynamic, with spatter and ash accumulating around vents leading to changes in the apparent size, shape, and position of vents.

A number of studies on Yasur have focused on the characteristics of strombolian activity and, in particular, its dynamism. Multi-vent basaltic volcanoes are known to exhibit vent-specific behaviours which can change through time, e.g., Salvatore et al. (2018) concerning Stromboli. Simons et al., (2020) discuss systematic changes in behaviour at individual vents within the southern crater at Yasur, with switching from bomb-rich (incandescent pyroclasts) through to ash-rich explosions. They also discuss conduit branching and the possibility of a common source bubble (i.e., gas slug) driving paired explosions from separate vents at Yasur, with the potential for diverging eruption styles at the vents being linked to cooling of the magma in the upper conduit sections. Spina et al., (2016), using infrasound, observed two distinct styles of degassing (puffing, which was observed as near-constant; and strombolian explosions), indicating that their behaviours were decoupled, while Meier et al., (2016) highlight the ash-rich and ash-poor (or bomb-rich), respectively styles and their similarity to those of Stromboli (Gaudin et al., 2014b; Patrick et al., 2007; Ripepe et al., 2005; Ripepe and Marchetti, 2002; Taddeucci et al., 2012). Kremers et al. (2013) were able to calculate the lengths of gas slugs generating the strombolian explosions on Yasur, ranging from 59 to 244 m, with mean and median values of 112 m and 103 m, respectively.

Regarding SO_2 fluxes, Bani and Lardy (2007), measured values ranging 2.5 to 17.2 kg s^{-1}, with a mean of 7.9 kg s^{-1} from April 2004 to November 2005 based on differential optical absorption spectroscopy (DOAS) traverses. Bani et al. (2012) published additional data collected between August 2007 and December 2008, with fluxes of 1.3 to 11.1 kg s^{-1}, with a mean and median of 7.2 kg s^{-1} and 7.1 kg s^{-1} respectively. Métrich et al., (2011) measured a mean of 8.0 ± 3.8 kg s^{-1} across four days of traverses in October 2007. Finally, Carn et al., (2017) report a satellite derived range of 6.8 to 23.3 kg s^{-1} measured between 2000-2015, with a mean and median of 16.3 kg s^{-1} and 19.2 kg s^{-1} respectively. With these values we emphasise the need to treat comparisons in gas flux data between different periods of observations carefully, and that these results may, arising from discrete campaigns such as presented in this study, not represent broader changes through time (or even match concurrent satellite derived estimates). Indeed, there are known issues associated with direct comparisons of satellite and ground-derived estimates of SO_2 outputs (Campion et al., 2012; McCormick et al., 2014). Note that, all of the above are combined passive plus explosive estimates, here, we use UV cameras to derive the first direct measurements of explosive gas masses.

3. UV Camera methods

Low-cost Raspberry Pi ultraviolet (UV) camera systems (the 'PiCams') were used to measure volcanic SO_2 outgassing, ((Wilkes et al., 2017, 2016); in this case the units were modified to include 'PiJuice' hardware and software (https://github.com/PiSupply/PiJuice) to provide power to the Raspberry Pi boards which are at the heart of the camera system. The PiJuice units provide continuous supplies of power via lithium-polymer mobile phone batteries, which can be recharged using solar panels. In the field, we used both 1600 mAh and 2300 mAh batteries and found that with continuous solar charging (implementing 40 W solar panels for each Pi board) this configuration readily enabled field data acquisition for at least 6-7 hours per day in

this location. This camera setup also involved omitting the GPS module included in the prior generation of the Pi Cam system, which automatically provided time synchronisation for the Raspberry Pi computers on start-up. Instead, in this configuration, GPS time synchronisation was performed manually via the command line, expedited by the PiJuices' on board real-time-clock. The PiCam camera systems were furthermore equipped with two Edmund Optics Inc. filters (of full width at half maximum - 10 nm), centred around 310 and 330 nm, respectively, one for each lens, corresponding to spectral regions where SO_2 does and does not absorb incident UV radiation. As detailed further elsewhere, UV imaging systems in volcanic gas monitoring are predicated upon contrasting image intensities in these two wavebands, to isolate absorption in the image cause by sulphur dioxide absorption; for further details please see: (Gliß et al., 2017; Kantzas et al., 2010; Kern et al., 2015; McGonigle et al., 2017; Mori and Burton, 2006; Platt et al., 2015).

Two separate camera systems (Camera 1 and Camera 2) were set up viewing the plume simultaneously (enabling assessment of error and multiple plume angles simultaneously), from a position southwest of the summit crater from a treehouse (Treehouse site, ~1900 m from the plume) at the Jungle Oasis, on 6th and 7th July, and from another, on the ash plain (Ash Plain site, ~2300 m from the plume) to the north-northwest on 8th and 9th July (see Figure 2). The UV cameras were also operated on the 11th July, however, in this case inclement weather and grounding of the plume prevented reliable data processing. Note that all times and dates reported here are UTC. During the measurement days, the plume direction varied from west to northwest, with dry and predominantly cloud-free weather (bar a brief period of rain on the 9th of July). Of the five days on which measurements were attempted, we acquired high quality data on four of the days, amassing 16 hours of high quality imagery overall across these days.

The camera images were captured with acquisition rates ranging 0.5 – 0.25 Hz, with additional collection of clear sky images prior to the plume sequences' capture, which are required in the processing routine to account for vignetting effects. Dark images were acquired per sequence too, to enable subtraction out of dark noise. We furthermore conducted frequent calibrations using gas cells with known SO_2 column densities (0 ppm m, 412 ppm m, and 1613 ppm m; with a manufacturer quoted error of 10%) between measurement sequences, not more than every 1-1.5 hours, with more frequent calibration when light conditions changed more rapidly. The data were then processed following the commonly applied protocols, already extensively referenced in the literature (D'Aleo et al., 2016; Kantzas et al., 2010; Kern et al., 2014; McGonigle et al., 2017) e.g., involving aligning images; selecting a clear sky background region; and choosing a plume cross-section along which to determine integrated column amounts (ICA), before multiplying by plume speed to calculate flux. For the resulting flux data time series, we determined data normality statistically with the Kolmogorov-Smirnov normality test. The data were all non-normally distributed, therefore the median was used in the further calculations, detailed below. However, we quote both mean and median values, heretofore.

One of the goals of this study was to attempt to discriminate between degassing from the different vent areas. However, it was not possible to do this rigorously and at all times, given

that changes in wind shear and crater derived eddying led to time varying separation/overlap of these individual plumes (Pering et al., 2019b; Tamburello et al., 2013), creating difficulties in resolving emissions from the individual vents. Indeed, the plume predominantly appeared well-mixed on emergence from the summit crater (Figure 2c). However, at times, the view from the ash plain site did allow us to identify gas pulses from the individual sources, likely associated with explosions, where distinct gas clouds from individual craters could be clearly spatially resolved (Figure 2d).

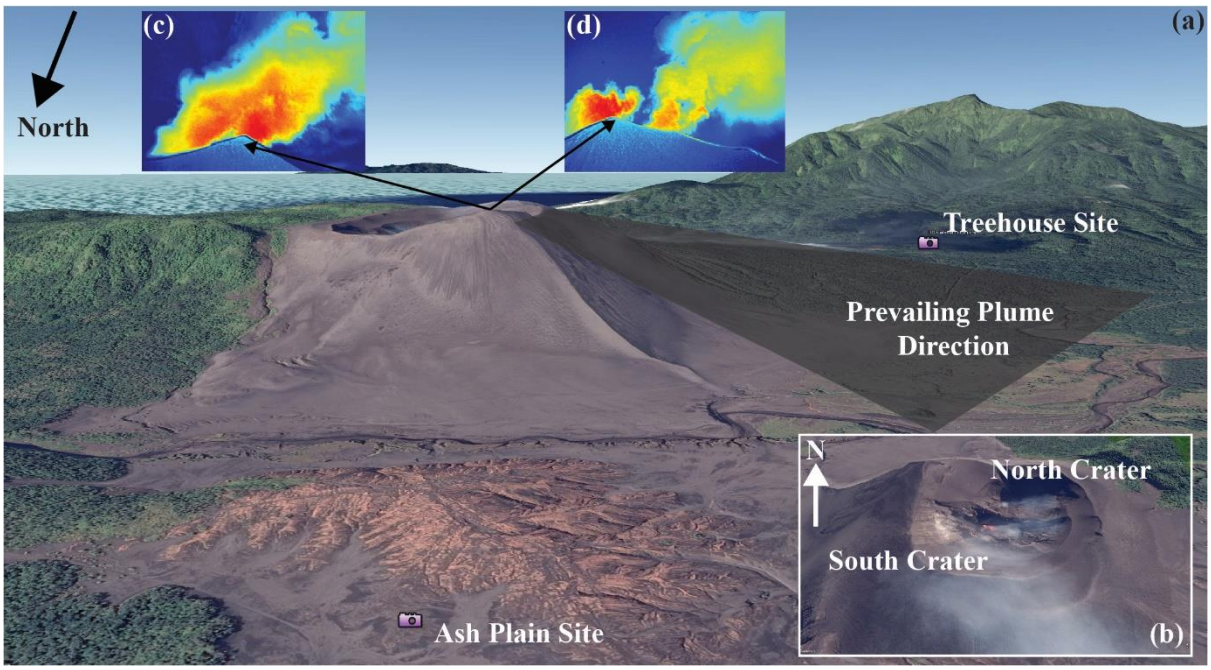

Figure 2: (a) An elevation-based perspective of the low summit of Yasur volcano, along with measurement positions and prevailing plume transport direction with inset (b) showing a close-up of the summit crater. In (c) there is a typical view of the plume with red colours representing higher concentrations of SO_2, demonstrating mixing between gases from both crater areas, and (d) shows an example of where it was possible to differentiate between emissions from both craters. Imagery is from Google Earth®.

3.1. Particle Image Velocimetry (PIV) for plume velocity determination.

One of the most important, and yet readily overlooked error in UV camera image analysis is associated with plume velocity determination, for which three main methods are commonly used: cross-correlation (McGonigle et al., 2005; Williams-Jones et al., 2006), optical-flow (Gliß et al., 2017; Kern et al., 2015; Peters et al., 2015; Peters and Oppenheimer, 2018), and manual tracking (Ilanko et al., 2019). Indeed, the optimal method will largely be determined by the manifested plume conditions, as no single method is ideally suited to all situations. Manual tracking can be suitable for stable plumes travelling at slow velocities, or for measurements at greater distances from the plume, where cross-correlation and optical-flow are less desirable, as the plume is more dilute and fewer pixels containing SO_2 are available for the analysis. Cross-correlation could be preferable for broadly homogenous plumes that are

well-mixed and present little turbulence (e.g., whereby eddying can cause SO_2 within parts of the plume to travel backwards relative to the bulk plume vector of motion e.g., the wind direction); and optical-flow may be better with high velocity plumes, where the velocity field over the plume profile is non-constant, e.g., due to pulsed gas outputs from craters, associated with strombolian explosions or puffing (Liu et al., 2019; Peters et al., 2015).

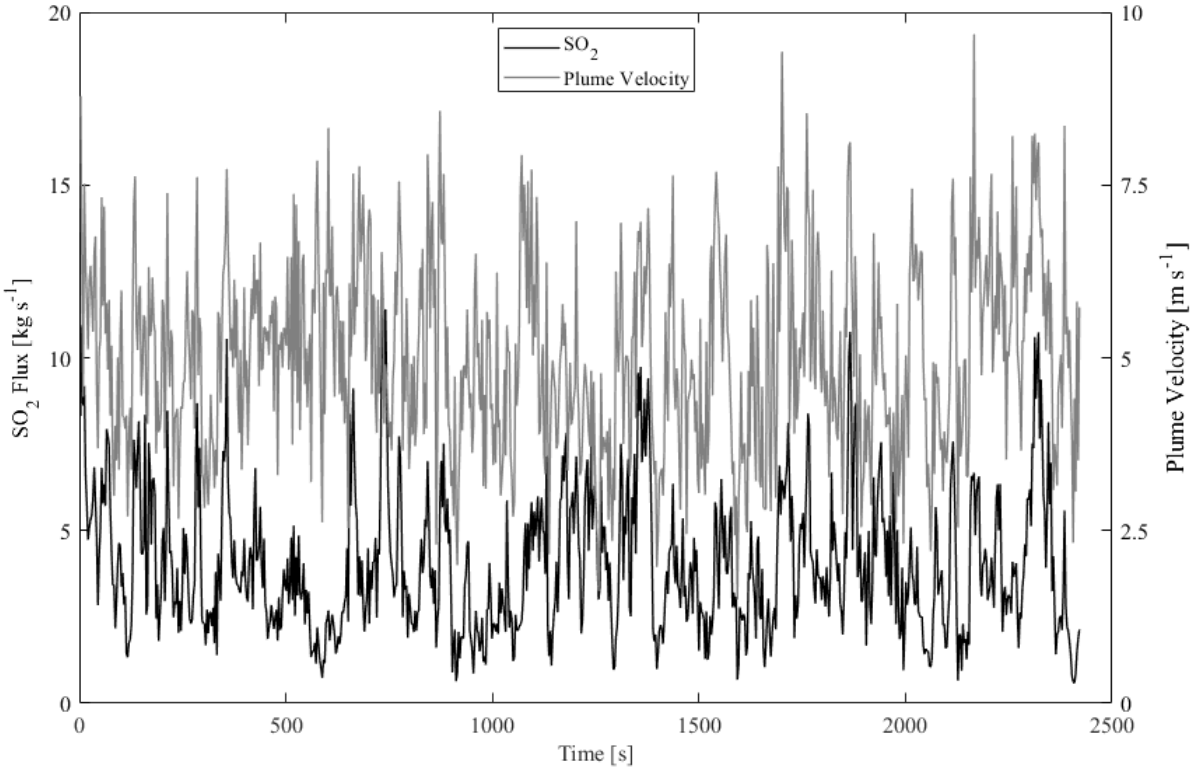

Figure 3: Example plume velocity and SO_2 fluxes for a period on the 7th July 2018, where clear accelerations in plume velocities are evident, corresponding to strombolian explosions.

Here, we encountered difficulties in using these traditionally applied methods, and in particular needed a less time consuming mechanism than manually tracking pulses of gas in such a large dataset. Indeed, cross-correlation sometimes failed, likely as a result of turbulent motion in the plume, and furthermore this approach does not cope well with transient increases in gas velocity, associated with impulsive gas release during strombolian explosions; hence this method is probably the least favourable in this context. In addition, a lack of structure in the plume appeared to lead to the failure of optical flow algorithms (Gliß et al., 2017; Peters et al., 2015; Wilkes et al., 2017). We therefore instead adopted the use of Particle Image Velocimetry (PIV) for plume velocity determination, as briefly discussed in Kern et al. (2015). Previous use of PIV in a volcanic context has included tracking of lava lake velocity at Masaya (Pering et al. 2019) and similar to the pyroclast tracking velocimetry of (Gaudin et al., 2014a, 2014b). Here, we used PIVlab, a user-friendly MATLAB toolbox and app (Thielicke, 2014; Thielicke and Stamhuis, 2014). PIV works by comparing image pairs in sequences and looking for differences between them through two methods: direct cross-correlation and through the correlation of Fourier transforms. Both of these are conducted on integration areas (here we used three), with decreasing size on each pass. The end result is a velocity grid for the whole

plume image, similar to those produced during the application of optical flow (Gliß et al., 2017; Peters et al., 2015). We found that using PIV we were able to identify velocity differences in relatively homogenous plumes (i.e., with quasi-uniform SO_2 distribution across most of the plume, except during strombolian explosions). PIV was used to extract velocity components corresponding to each image pixel, along, and perpendicular to, the integration line used in the ICA determination. In this case, rather than using a single plume speed vector, perpendicular to the integration line, therefore, the plume speed vectors per pixel were multiplied by the pixel's SO_2 column amount, and these sums were then integrated over the plume profile (see Figure 3). The PIV analyses show temporal and spatial variability in plume speed, therefore, capturing a heterogeneity which is a real feature of the plume motion, yet not captured by cross-correlation or manual tracking. We report error for PIV analysis as the distance along the integration line at the plume range, corresponding to each pixel, divided by the lowest image capture frequency; for the ash plain this equates to an error of 2 ± 0.3 ms^{-1} or ~ ±15%, and for the treehouse site an error of 5 ± 0.6 ms^{-1} or ~9±%. These are based on typical plume speeds for each site.

3.2. Estimation of a total UV Camera Measurement Error

Error is an important aspect of all UV camera measurements. Here, we highlight the range of possible error sources, and perform additional analyses on our data pertaining, specifically to calibration curve drift, plume orientation, and plume distance. The final determined values for error are our best possible estimates on the basis of the available information and protocols applied in-the-field, which, wherever possible, were designed to minimise error.

Campion et al., (2015) investigated the effects of light dilution at a range of volcanic targets and identified a broad range of ~10-60% underestimation in SO_2 content for measurement positions varying between 2.1 km and 6.5 km of the plume, and a variety of encountered conditions e.g., ranging hazy through to very clear. Light dilution has a larger effect during hazier conditions, which were not present during our successful measurement days. Ilanko et al., (2019), calculated that at ~10.3 km distance from the plume (during clear conditions) SO_2 fluxes could be underestimated by 2.5 times, and at 4.25 km by 1.5 times (which would correspond to ~1.18 times [18%] at our maximum distance of 2300 m). It is important to note that light dilution estimates are specific to each measurement location and given our range of distances to the plume and clear measurement conditions we suggest that error relating to light dilution is <+20%. We therefore take the value of +20% as our maximum light dilution error (i.e., light dilution causes underestimation). We also note that the plume was not optically thick, except following ash-rich strombolian explosions. Unfortunately, exact errors due to ash are currently not quantifiable, but we can state that ash within the plume will likely lead to an underestimation of values (Kern et al., 2013; Tamburello et al., 2012).We attempted to minimise this error by integrating away from the summit area, where the plume is visibly less ash rich, and more transparent. We also further note that the peaks from strombolian explosions are well defined within the resulting dataset (Figure 3).

Table 1: A summary of error sources, values, including short comments and total RMS error.

	Treehouse	**Ash Plain**	**Comments**
Distance	1900 m	2300 m	-
Description	**Error**	**Error**	-
Light Dilution	+20%	+20%	Underestimation only, low given plume proximity.
Gas Cell Concentration	±10%	±10%	Manufacturer quoted
Calibration drift	±15%	±15%	Changing calibration conditions (see text)
Plume Velocity	±9	±15%	Based on pixel size (see text)
Plume Direction	±5%	±5%	Based on coincident UV camera data
Plume Distance	±18%	±18%	Based on plume deviation of 200 m.
Ash content	-	-	Underestimation, not quantifiable
RMS Error	-11.2% / +13.9%	-12.2% / +14.7%	Note the higher error related to underestimation (positive error).

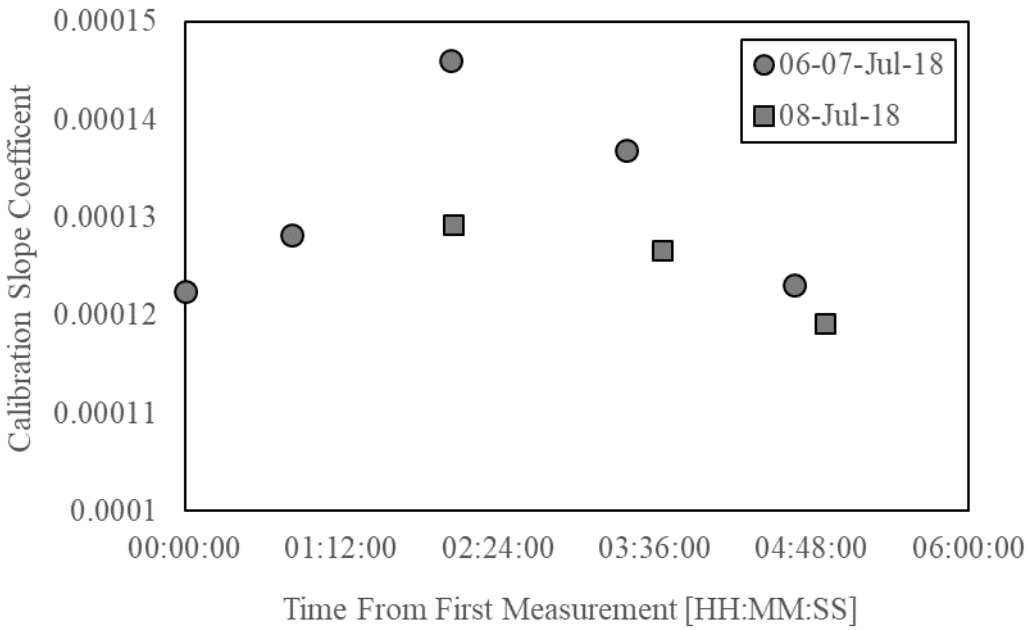

Figure 4: Example calibration slope coefficients from two days of data. Timings are from the time of the first calibration on each of these measurement days. Note that the data peaks towards solar noon.

Gas cell calibration will alter throughout the day based on position of the sun and changing illumination as a result of background clouds, with changes in gas-cell calibrations potentially leading to over-estimation in SO_2 column densities of up to 60% (Lübcke et al., 2013). Figure 4 shows the change in calibration slope coefficient (between regressions apparent absorbance coefficient and column density) throughout the day from time of first calibration (rather than using UTC), showing a variation from 1.22×10^{-4} to 1.46×10^{-4} in this parameter. When taking into account this characterised range in slope of 2.4×10^{-5}, and the broad assumption (for indicative illustration purposes) that there is a linear change between the first point and the

highest point (corresponding to maximum solar zenith angle) we arrive, over the 122 minutes between these points, at a value of 1.97 x 10^{-7} increase in slope coefficient per minute. This would equate to a potential error of ~ 0.16% per minute, which expanded over an hour could become 9.6% - or, for our maximum inter-calibration interval of ~95 minutes, an error of 15.2%. It is possible therefore that any underlying trends in apparent gas emission rates below these thresholds are not differentiable from this error, i.e., an increase or decrease in flux at a rate of <~0.16% per minute. We suggest therefore that errors from cell calibration (notwithstanding the ~±10% manufacturer quoted cell content error) amount to a maximum of ~±15% for our measurement period.

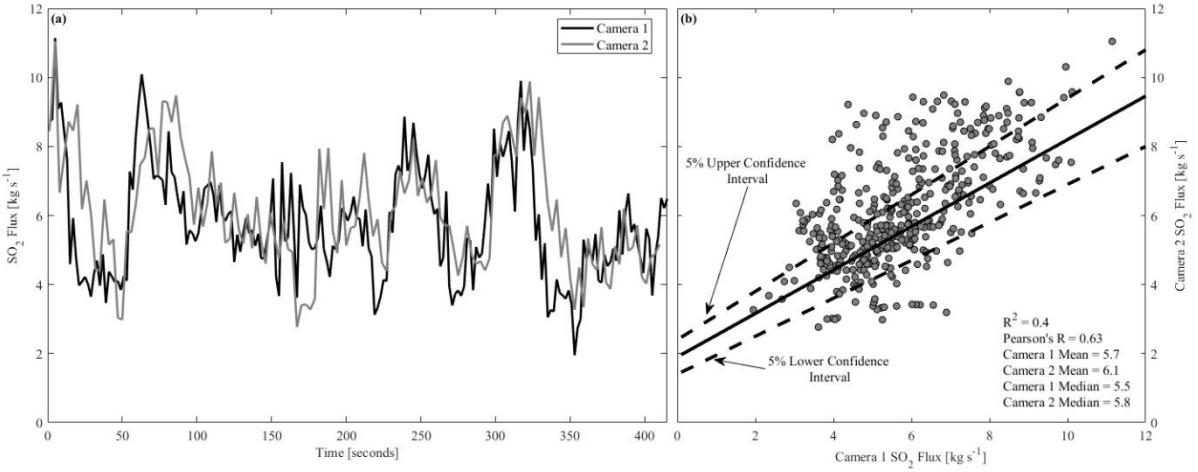

Figure 5: (a) Example period of overlapping data from two separately acquiring synchronous cameras, viewing the plume from slightly different orientations. One dataset has been shifted by the lag value which generated the maximum correlation coefficient, following cross-correlation between the two series, in an attempt to best temporally match the data. Note that there are differences in the magnitudes of peaks and troughs in the different dataseries, even when shifted relative to one another in this way, due to smoothing or turbulence during plume movement through the atmosphere and the slightly different views of the units through the plume. In (b) a linear regression model ($R^2 = 0.4$) is shown, demonstrating the best fit between time series data from the two cameras, as well as confidence intervals. The statistical parameters are similar, but there are differences in peaks and troughs between the two datasets.

We used fixed distances of 1900 m and 2300 m from the camera to the plume for our retrieval calculations in the cases of data from the treehouse and ash plain sites, respectively. For the ash plain data, we determined, therefore that a 100 m error in plume distance leads to a < 5% difference in computed gas masses across the plume cross section (with underestimation in this distance corresponding to underestimation in gas mass), and a 200 m error in distance to < 9% error. Comparisons of the same test dataset with different velocities in PIV analyses showed variations from 1 – 7 % with 100 m distance to plume error and 5 – 11% in the 200 m case. The combined effect of these distance uncertainties on mass and velocity gives a 7-10% error in fluxes for 100 m distance to plume error, and 16-18 % for 200 m. We therefore take the maximum value here of ~18% and apply this conservatively, to our entire dataset. As an example of how distance errors might affect our data, during the measurement period on 9th

July, the plume visually appeared to drift closer to the camera, which could have caused the retrieved SO_2 fluxes to have been underestimated.

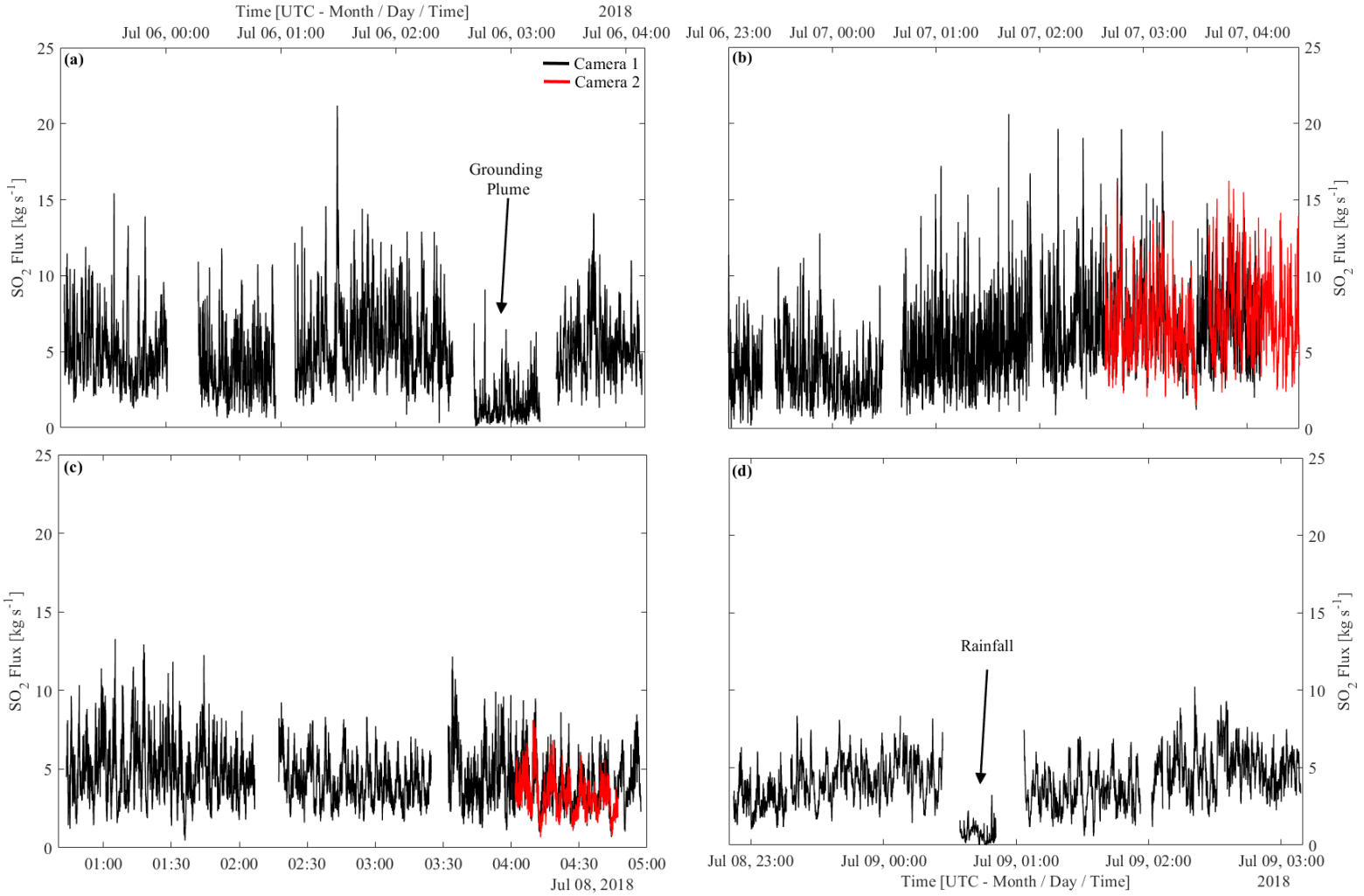

Figure 6: (a) through (d) show retrieved gas fluxes for all the image data captured during the observation period; also highlighted are periods where the plume was grounded in (a) and heavy rainfall was encountered in (d).

Given changes in plume direction, the orientation with which the integration line bisects the plume is also relevant in consideration of measurement uncertainty (Klein et al., 2017). To investigate this, we use overlaps between data from two synchronously acquiring cameras (Figure 5), which had slightly different plume views and hence integration line orientations relative to the plume geometry, simulating the time dependent effect of the plume vector moving, in response to changing wind conditions, with respect to a fixed integrated column amount line. In this case the two datasets were cross-correlated and shifted by the lag corresponding to the maximum correlation to account for different transport times from the source to the two cameras' different integration lines. The calculated difference in flux retrieval from the two units, based on comparing the acquired median values per unit is ~±5%.

In addition, we also report computed flux data in Figure 6 (which documents the retrieved data from the entire campaign) during periods when the plume grounded, e.g., the integration line

could not cover the entire plume cross section, as well as episodes of heavy rainfall. During these periods, median SO_2 fluxes were underestimated significantly by ~4.3-4.4 and 5.6-7.3 times, respectively, based on comparison with median values of retrieved fluxes either side of these episodes. Whilst the data captured under these circumstances were not used in the foregoing analysis, nor considered representative of the volcanic outgassing, they are reported here, to illustrate the significant error these effects give rise to.

Table 2. A summary of measurement durations and SO_2 flux statistics for our measurement period.

Date (UTC)	**05-06/07/18**	**06-07/07/18**	**08/07/18**	**08-09/07/18**
Date (Local)	**06/07/18**	**07/07/18**	**08/08/18**	**09/08/18**
Time series duration (hh:mm)	4:15	04:42	03:54	03:33
Total time (hh:mm)	05:01	05:31	04:14	04:17
Mean (kg/s)	5.2	5.5	4.5	4.1
Median (kg/s)	4.7	5.1	4.2	4.0

4. Results and Discussion

4.1 SO_2 Fluxes and Manually Derived Explosion Masses

Time series gas fluxes are shown in Figure 6, with a summary of daily statistics in Table 1. The median flux across the four days of measurements was 4.5 $kg \cdot s^{-1}$ and the mean was 4.9 $kg \cdot s^{-1}$, reflecting the peaks in SO_2 flux associated with frequent strombolian explosions. This corresponds to a daily median and mean of 389 and 423 $t \cdot d^{-1}$ across the measurement period. Daily statistics are given in Table 1: median SO_2 fluxes (calculated using the camera providing the bulk of each day's data) ranged between 4.0 – 5.1 $kg \cdot s^{-1}$ across the measurement days. The daily means ranged 4.1 to 5.5 $kg \cdot s^{-1}$. The timeseries data are suggestive of gradual changes in background gas release trends over several hours, but it is not clear whether these correspond to real degassing changes or some drift based error. A shift in activity is, however, plausible based on the observation of large strombolian explosions with visible ballistics and shockwaves, particularly on 8th and 9th July, when lower fluxes were measured.

The SO_2 gas masses released per explosion were calculated following the method of Tamburello *et al.*, (2012), by integrating over the timeframe of the corresponding explosive pulse in the gas flux timeseries to determine the total SO_2 released during the event. Although, a key difference here is that the source of the strombolian explosions were not visible within the imagery (i.e., the vents were concealed behind the crater rim, from the vantage points of the measurement locations). We use two methods to determine when explosions occurred within the UV camera imagery: firstly, when gas pulses in the camera images are observed to originate and visibly accelerate above the rim of the summit crater (see Figure 1a); secondly, where gas burst traces are manifested in the flux time series, showing the characteristic coda detailed in Pering *et al.*, (2016). Note here that this assessment is therefore likely to lead to an underestimation in the reported frequency of explosive events, and therefore a lower boundary for the explosive:passive degassing ratio, nevertheless the absolute explosive gas masses per event to provide an absolute reference for useful comparison to literature values for other volcanoes; see Table 3 for a summary of our extracted passive and explosive gas observations

per measurement day. Overall, we extracted SO_2 masses for 135 explosions, across the five UTC dates. We show an increasing mean mass from 6th to 9th July, which corresponds to visual observations of more powerful explosions on 8th and 9th July.

Table 3: A breakdown of daily SO_2 explosion mass data. Also displayed are ratio data in percentage terms, concerning the portioning of gas fluxes between passive and explosive release. Lower and Upper ratios refer to the ranges indicated in determined active molar ratios by (Woitischek et al., In Review; Table 3 - CO_2/SO_2 = 2.85 ± 0.17; H_2O/SO_2 = 315 ± 71.8; SO_2/HCl = 1.6 ± 0.22).

Date	**05/07/2018**	**06/07/2018**	**07/07/2018**	**08/07/2018**	**09/07/2019**	**Total**
Explosions Counted	8	43	39	36	9	**135**
Data	**05/07/2018**	**06/07/2018**	**07/07/2018**	**08/07/2018**	**09/07/2019**	**Mean**
SO_2 Min (kg)	10.2	8.9	8	12	10	**9.8**
SO_2 Mean (kg)	26.9	22.1	27	39	45	**32.0**
SO_2 Max (kg)	64.1	44.9	62	81	69	**64.2**
Passive %	66	64	70	78	68	**69**
Explosive %	34	36	30	22	32	**31**
Lower Ratios	**05/07/2018**	**06/07/2018**	**07/07/2018**	**08/07/2018**	**09/07/2019**	**Mean**
Total – Min (kg)	712	625	575	822	721	**691**
Total – Mean (kg)	1884	1550	1892	2713	3164	**2241**
Total – Max (kg)	3020	3148	4370	5678	4813	**4206**
Middle Ratios	**05/07/2018**	**06/07/2018**	**07/07/2018**	**08/07/2018**	**09/07/2019**	**Mean**
Total – Min (kg)	940	824	759	1084	952	**912**
Total – Mean (kg)	2486	2046	2497	3579	4175	**2957**
Total – Max (kg)	5929	4153	5767	7493	6350	**5938**
Upper Ratios	**05/07/2018**	**06/07/2018**	**07/07/2018**	**08/07/2018**	**09/07/2019**	**Mean**
Total – Min (kg)	1167	1024	942	1347	1182	**1132**
Total – Mean (kg)	3088	2541	3102	4446	5186	**3673**
Total – Max (kg)	7365	5159	7163	9307	7888	**7376**

The range of explosive SO_2 masses at Yasur of 8 – 69 kg (mean 32 kg) are similar to those of Tamburello et al., (2012) at Stromboli (2 – 55 kg; mean of 20 kg); but higher than those at Etna during mild strombolian activity determined by Pering et al., (2015), which ranged: 0.1 – 14 kg. Woitischek et al., (In Review) present gas ratio data (SO_2, H_2S, H_2O and CO_2) for Yasur, derived from a combined Fourier transform infrared spectroscopy (FTIR) and Multi-GAS study, in an observation window, period following our observations, with a brief overlap. The authors separated passive from explosive molar ratios, determining active (strombolian) ratios of: CO_2/SO_2 = 2.85 ± 0.17; H_2O/SO_2 = 315 ± 71.8; SO_2/HCl = 1.7 ± 0.22. From these we can estimate total slug masses at Yasur which are highlighted in Table 3. Our mean total gas mass

per explosion based on the mean measured active degassing ratios, is: ~2960 kg, ranging 910 – 5940 kg. These compare with a range of 170 – 1674 kg for Pacaya (Dalton et al., 2010); whilst at Stromboli values range 44 to 238 kg according to Barnie et al. (2015) and 2 to 1425 kg as determined by Delle Donne et al. (2016).

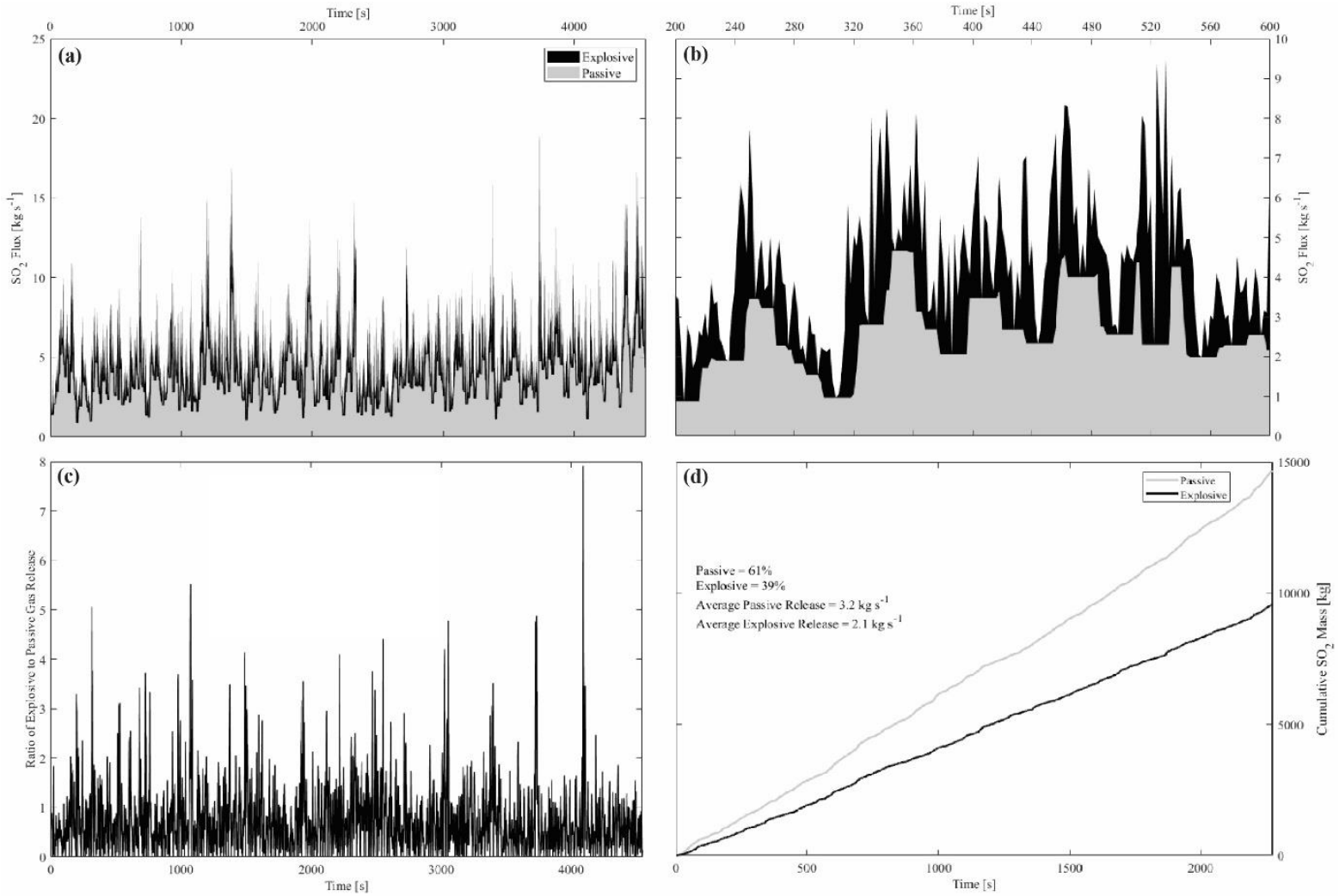

Figure 7: (a) Separation of passive and explosion gas release for a period on the 7th July; (b) a zoomed illustration of the simple statistical moving minimum based model, showing oscillation in background passive degassing overtopped by explosive contributions; (c) the ratio of passive to explosive degassing; and (d) a cumulative plot showing the division between passive and explosive gas release, here passive and explosive release have been cumulatively summed to show the change through time at the sampling frequency. The passive to explosive ratio is then the ratio of the final sum of gas release.

4.2. Simple Statistical Separation of Passive and Explosive Degassing

Other workers have studied the ratios of explosive to passive release during strombolian explosions on Stromboli (Tamburello et al., 2012) and Etna (Pering et al., 2015). Here, we attempt to expand on this by using a simple statistical measure involving the moving minimum, to estimate the passive release of gas through time, which, when subtracted from total flux,

provides an approximate estimate of passive vs. explosive release. For an example period (Figure 7) we highlight the moving minimum, which is set to a window size of 20 s, which is generally the characteristic timeframe of large peaks and troughs associated with strombolian explosions (Pering et al., 2016). In this instance, a moving minimum over this window proved best, given the higher frequency of explosive events; however, with a greater timeframe between events, the moving median may be a better measure. We also prefer this statistical estimation technique over using our estimated SO_2 masses, given that the latter required manual selection of strombolian explosions. This simple moving minimum approach could be readily and simply automated for routine monitoring of activity from strombolian explosion producing volcanic systems.

Resulting day-by-day estimates of passive:explosive degassing based on this approach are detailed in Table 3, with a mean of 69% passive to 31% explosive over all the measurement days. These are in line with those measured at Stromboli: 77% passive to 23% explosive (termed active which also includes puffing); and Etna, 67% passive to 33% explosive (Pering et al., 2015). These datasets serve to illustrate the dominant role of passive degassing at volcanoes with strombolian eruptions. On the 8th July we calculated a higher passive contribution at 78%. At the same time, we measure higher SO_2 masses, but lower overall SO_2 fluxes. This could indicate a magmatic system that is cooling or capped by a thickening plug (Polacci et al., 2012; Simons et al., 2020), therefore becoming less permeable for passive gas release, therefore requiring higher gas masses to drive explosions, which would be correspondingly more powerful, in line with our visual observations.

4.3.Models of gas slug behaviour

Using our determined values for total slug mass, we can estimate slug lengths using the static pressure model of (Del Bello et al., 2012). We use fixed values of 2600 kg m^3 and 1000 Pa s^{-1} for density and viscosity, respectively, with an atmospheric pressure of 101,325 Pa. The only parameter we vary in the model conduit diameter, which we step, in 1 m increments, from 3 m to 7 m. We also use only the mean explosive ratios and masses (and not the range obtained when including error) for simplicity. Our results are summarised in Table 4. We therefore determine slug lengths ranging 188 – 609 m (median and mean of 347 m and 366 m, respectively) for a conduit diameter of 3 m, however, this reduces to 76 – 260 m (median and mean of 146 and 154 m respectively) for a conduit diameter of 7 m. Kremers et al. (2013) calculated distinctly lower values of 59 – 244 m for Yasur using seismo-acoustic data, and it would therefore seem that a larger conduit diameter may be more plausible for this target, perhaps at depth and prior to any conduit bifurcation or splitting at shallow depths (Simons et al., 2020). It should also be noted that the H_2O/SO_2 ratios used in this work are high and variable, i.e., large ranges (Woitischek et al., In Review). As water is the gas contributing most to the mass of the slug, it is likely that our determined masses are an overestimation. In addition, others have shown that UV camera-derived masses can be over-estimated compared with infrasound-derived masses (Dalton et al., 2010).

Table 4: A summary of slug volumes and calculated slug lengths using the model of Del Bello et al. (2012).

Statistic	Slug Volume (m^3)	D = 3 m	D = 4 m	D = 5 m	D = 6 m	D = 7 m
Min	4286	188	139	110	90	76
Median	14055	347	259	205	170	146
Mean	15556	366	272	217	180	154
Max	42337	609	455	364	303	260

5. Summary and Conclusions

In this work we highlight the utility of using low-cost solar-powered Raspberry Pi UV cameras for prolonged field campaigns to capture volcanic degassing data. We were able to continuously image the volcanic plume to yield both velocity, using a PIV method (Thielicke, 2014; Thielicke and Stamhuis, 2014), and SO_2 fluxes over periods of several hours per day, at temporal resolutions of up to 0.5 Hz with brief pauses for calibration. Our determined SO_2 fluxes with means 4.1-5.5 kg s^{-1} (medians from 4.0-5.1 kg s^{-1}) are within the ranges of those measured previously at Yasur using ground based methods of 2.5 to 17.2 kg s^{-1} (Bani et al., 2012; Bani and Lardy, 2007). We further highlight SO_2 masses of strombolian explosions of 8-81 kg, showing these to be of similar magnitude to events at Stromboli of 2 – 55 kg (Tamburello et al., 2012). By using a simple statistical measure we estimate that passive degassing, at 69% of the total gas discharge, is the dominant mode of degassing at Yasur, compared to 31% explosive. These data from our brief observation period are suggestive that periods of lower gas output could lead to conduit sealing and more visibly violent explosions, however, a longer dataset would be needed to test this hypothesis substantively. By combining SO_2 explosion masses with gas ratios (Woitischek et al., In Review) we determined mean total explosion masses of ~910-5940 kg, which correspond to slug lengths, using the model of Del Bello et al. (2012), of ~76-260 m, assuming a conduit diameter of ~7 m. Smaller conduit diameters lead to far longer slug lengths, ~188-600 m at 3 m diameter, larger than those estimated previously of ~59 – 244 m (Kremers et al., 2013) based on analysis of volcano-acoustic data.

This work and others (Ilanko et al., 2019) have further highlighted the utility of using a multiple UV camera approach to performing gas measurements at volcanoes, particularly when considering errors in the data, as well as introducing the PIV method for plume flux determination, which we suggest could be robustly used across a variety of plume conditions. The data presented here represent an important addition to our gas data based characterisation of the spectrum of strombolian activity across the globe.

6. Acknowledgements

We would like to thank the Vanuatu Meteorology and Geo-hazards Department for permission to conduct this fieldwork, Kelson and Joyce Hosea for their hospitality at the Jungle Oasis, and Roger for his assistance in the field. J.W and M.E .were supported by the Natural Environment Research Council (grant number NE/L002507/1), by the postgraduate travel funds received

from Fitzwilliam College, by the Elspeth Matthews grant given by the Royal Geological Society, by the Mary Euphrasia Mosley, Sir Bartle Frere and Worts travel fund report given by the University of Cambridge and by the Exzellenzstipendium received by WKO. A.A. acknowledges funding support from the Alfred P. Sloan Foundation via the Deep Carbon Observatory (UniPa-CiW subcontract 10881-1262) and from MIUR (under grant n. PRIN2017-2017LMNLAW). T.D.P. acknowledges the support of the Royal Society (RG170226). T.I. is a Commonwealth Rutherford Fellow, funded by the UK government. A.McG. acknowledges support from the Rolex Institute.

7. References

Aiuppa, A., Coco, E. Lo, Liuzzo, M., Giudice, G., 2016. Terminal Strombolian activity at Etna's central craters during summer 2012: The most CO 2-rich volcanic gas ever recorded at Mount Etna. Geochemical.

Aiuppa, A., Federico, C., Giudice, G., Gurrieri, S., 2005. Chemical mapping of a fumarolic field: La Fossa Crater, Vulcano Island (Aeolian Islands, Italy). Geophys. Res. Lett. 32, L13309. https://doi.org/10.1029/2005GL023207

Bani, P., Lardy, M., 2007. Sulphur dioxide emission rates from Yasur volcano, Vanuatu archipelago. Geophys. Res. Lett. 34. https://doi.org/10.1029/2007GL030411

Bani, P., Oppenheimer, C., Allard, P., Shinohara, H., Tsanev, V., Carn, S., Lardy, M., Garaebiti, E., 2012. First estimate of volcanic SO 2 budget for Vanuatu island arc. J. Volcanol. Geotherm. Res. 211–212, 36–46. https://doi.org/10.1016/j.jvolgeores.2011.10.005

Barnie, T., Bombrun, M., Burton, M.R., Harris, A., Sawyer, G., 2015. Quantification of gas and solid emissions during Strombolian explosions using simultaneous sulphur dioxide and infrared camera observations. J. Volcanol. Geotherm. Res. 300, 167–174. https://doi.org/10.1016/j.jvolgeores.2014.10.003

Barth, A., Edmonds, M., Woods, A., 2019. Valve-like dynamics of gas flow through a packed crystal mush and cyclic strombolian explosions. Sci. Rep. 9, 821. https://doi.org/10.1038/s41598-018-37013-8

Battaglia, A., Bitetto, M., Aiuppa, A., Rizzo, A.L., Chigna, G., Watson, I.M., D'Aleo, R., Juárez Cacao, F.J., de Moor, M.J., 2018. The Magmatic Gas Signature of Pacaya Volcano, With Implications for the Volcanic CO_2 Flux From Guatemala. Geochemistry, Geophys. Geosystems 19, 667–692. https://doi.org/10.1002/2017GC007238

Blackburn, E.A., Wilson, L., Sparks, R.S.J., 1976. Mechanisms and dynamics of strombolian activity. J. Geol. Soc. London. 132, 429–440. https://doi.org/10.1144/gsjgs.132.4.0429

Branca, S., Del Carlo, P., 2005. Types of eruptions of Etna volcano AD 1670-2003: Implications for short-term eruptive behaviour. Bull. Volcanol. 67, 732–742. https://doi.org/10.1007/s00445-005-0412-z

Burton, M., Allard, P., Mure, F., La Spina, A., 2007. Magmatic Gas Composition Reveals the Source Depth of Slug-Driven Strombolian Explosive Activity. Science (80-.). 317, 227–230. https://doi.org/10.1126/science.1141900

Campion, R., Delgado-Granados, H., Mori, T., 2015. Image-based correction of the light dilution effect for SO2 camera measurements. J. Volcanol. Geotherm. Res. 300, 48–57. https://doi.org/10.1016/j.jvolgeores.2015.01.004

Campion, R., Martinez-Cruz, M., Lecocq, T., Caudron, C., Pacheco, J., Pinardi, G., Hermans, C., Carn, S., Bernard, A., 2012. Space and ground-based measurements of sulphur dioxide emissions from Turrialba Volcano (Costa Rica). Bull. Volcanol. 74, 1757–1770. https://doi.org/10.1007/s00445-012-0631-z

Carn, S.A., Fioletov, V.E., Mclinden, C.A., Li, C., Krotkov, N.A., 2017. A decade of global

volcanic SO2 emissions measured from space. Sci. Rep. 7, 1–12. https://doi.org/10.1038/srep44095

Chouet, B., Dawson, P., Ohminato, T., Martini, M., Saccorotti, G., Giudicepietro, F., De Luca, G., Milana, G., Scarpa, R., 2003. Source mechanisms of explosions at Stromboli Volcano, Italy, determined from moment-tensor inversions of very-long-period data. J. Geophys. Res. Solid Earth 108, 2019. https://doi.org/10.1029/2002JB001919

D'Aleo, R., Bitetto, M., Delle Donne, D., Tamburello, G., Battaglia, A., Coltelli, M., Patanè, D., Prestifilippo, M., Sciotto, M., Aiuppa, A., 2016. Spatially resolved SO2 flux emissions from Mt Etna. Geophys. Res. Lett. 43, 7511–7519. https://doi.org/10.1002/2016GL069938

Dalton, M.P., Waite, G.P., Watson, I.M., Nadeau, P.A., 2010. Multiparameter quantification of gas release during weak Strombolian eruptions at Pacaya Volcano, Guatemala. Geophys. Res. Lett. 37. https://doi.org/10.1029/2010GL042617

Del Bello, E., Llewellin, E.W., Taddeucci, J., Scarlato, P., Lane, S.J., 2012. An analytical model for gas overpressure in slug-driven explosions: Insights into Strombolian volcanic eruptions. J. Geophys. Res. Solid Earth 117. https://doi.org/10.1029/2011JB008747

Delle Donne, D., Ripepe, M., 2012. High-frame rate thermal imagery of strombolian explosions: Implications for explosive and infrasonic source dynamics. J. Geophys. Res. Solid Earth 117, 1–12. https://doi.org/10.1029/2011JB008987

Delle Donne, D., Ripepe, M., Lacanna, G., Tamburello, G., Bitetto, M., Aiuppa, A., 2016. Gas mass derived by infrasound and UV cameras: Implications for mass flow rate. J. Volcanol. Geotherm. Res. 325, 169–178. https://doi.org/10.1016/j.jvolgeores.2016.06.015

Dibble, R.R., Kyle, P.R., Rowe, C.A., 2008. Video and seismic observations of Strombolian eruptions at Erebus volcano, Antarctica. J. Volcanol. Geotherm. Res. 177, 619–634. https://doi.org/10.1016/j.jvolgeores.2008.07.020

Firth, C.W., Handley, H.K., Cronin, S.J., Turner, S.P., 2014. The eruptive history and chemical stratigraphy of a post-caldera, steady-state volcano: Yasur, Vanuatu. Bull. Volcanol. 76, 1–23. https://doi.org/10.1007/s00445-014-0837-3

Garcés, M.A., Hagerty, M.T., Schwartz, S.Y., 1998. Magma acoustics and time-varying melt properties at Arenal Volcano, Costa Rica. Geophys. Res. Lett. 25, 2293–2296. https://doi.org/10.1029/98GL01511

Gaudin, D., Moroni, M., Taddeucci, J., Scarlato, P., Shindler, L., 2014a. Pyroclast Tracking Velocimetry: A particle tracking velocimetry-based tool for the study of Strombolian explosive eruptions. J. Geophys. Res. Solid Earth 119, 5369–5383. https://doi.org/10.1002/2014JB011095

Gaudin, D., Taddeucci, J., Scarlato, P., del Bello, E., Ricci, T., Orr, T., Houghton, B., Harris, A., Rao, S., Bucci, A., 2017a. Integrating puffing and explosions in a general scheme for Strombolian-style activity. J. Geophys. Res. Solid Earth 122, 1860–1875. https://doi.org/10.1002/2016JB013707

Gaudin, D., Taddeucci, J., Scarlato, P., Harris, A., Bombrun, M., Del Bello, E., Ricci, T., 2017b. Characteristics of puffing activity revealed by ground-based, thermal infrared imaging: the example of Stromboli Volcano (Italy). Bull. Volcanol. 79, 24. https://doi.org/10.1007/s00445-017-1108-x

Gaudin, D., Taddeucci, J., Scarlato, P., Moroni, M., Freda, C., Gaeta, M., Palladino, D.M., 2014b. Pyroclast Tracking Velocimetry illuminates bomb ejection and explosion dynamics at Stromboli (Italy) and Yasur (Vanuatu) volcanoes. J. Geophys. Res. Solid Earth 119, 5384–5397. https://doi.org/10.1002/2014JB011096

Gliß, J., Stebel, K., Kylling, A., Dinger, A., Sihler, H., Sudbø, A., Gliß, J., Stebel, K., Kylling, A., Dinger, A.S., Sihler, H., Sudbø, A., 2017. Pyplis–A Python Software

Toolbox for the Analysis of SO2 Camera Images for Emission Rate Retrievals from Point Sources. Geosciences 7, 134. https://doi.org/10.3390/geosciences7040134

Ilanko, T., Oppenheimer, C., Burgisser, A., Kyle, P., 2015. Cyclic degassing of Erebus volcano, Antarctica. Bull. Volcanol. 77, 56. https://doi.org/10.1007/s00445-015-0941-z

Ilanko, T., Pering, T., Wilkes, T., Apaza Choquehuayta, F., Kern, C., Díaz Moreno, A., De Angelis, S., Layana, S., Rojas, F., Aguilera, F., Vasconez, F., McGonigle, A., 2019. Degassing at Sabancaya volcano measured by UV cameras and the NOVAC network. Volcanica 2, 239–252. https://doi.org/10.30909/vol.02.02.239252

James, M.R., Lane, S.J., Corder, S.B., 2008. Modelling the rapid near-surface expansion of gas slugs in low-viscosity magmas. Geol. Soc. London, Spec. Publ. 307, 147–167. https://doi.org/10.1144/GSL.SP.2003.213.01.17

James, M.R., Lane, S.J., Wilson, L., Corder, S.B., 2009. Degassing at low magma-viscosity volcanoes: Quantifying the transition between passive bubble-burst and Strombolian eruption. J. Volcanol. Geotherm. Res. 180, 81–88. https://doi.org/10.1016/j.jvolgeores.2008.09.002

Jaupart, C., Vergniolle, S., 1989. The generation and collapse of a foam layer at the roof of a basaltic magma chamber. J. Fluid Mech. 203, 347–380. https://doi.org/10.1017/S0022112089001497

Jaupart, C., Vergniolle, S., 1988. Laboratory models of Hawaiian and Strombolian eruptions. Nature 331, 58–60. https://doi.org/10.1038/331058a0

Johnson, J.B., Aster, R.C., 2005. Relative partitioning of acoustic and seismic energy during Strombolian eruptions. J. Volcanol. Geotherm. Res. 148, 334–354. https://doi.org/10.1016/j.jvolgeores.2005.05.002

Johnson, J.B., Ripepe, M., 2011. Volcano infrasound: A review. J. Volcanol. Geotherm. Res. 206, 61–69. https://doi.org/10.1016/J.JVOLGEORES.2011.06.006

Kantzas, E.P., McGonigle, A.J.S., Tamburello, G., Aiuppa, A., Bryant, R.G., 2010. Protocols for UV camera volcanic SO2 measurements. J. Volcanol. Geotherm. Res. 194, 55–60. https://doi.org/10.1016/j.jvolgeores.2010.05.003

Kern, C., Lübcke, P., Bobrowski, N., Campion, R., Mori, T., Smekens, J.-F., Stebel, K., Tamburello, G., Burton, M., Platt, U., Prata, F., 2015. Intercomparison of SO2 camera systems for imaging volcanic gas plumes. J. Volcanol. Geotherm. Res. 300, 22–36. https://doi.org/10.1016/j.jvolgeores.2014.08.026

Kern, C., Sutton, J., Elias, T., Lee, L., Kamibayashi, K., Antolik, L., Werner, C., 2014. An automated SO2 camera system for continuous, real-time monitoring of gas emissions from Kīlauea Volcano's summit Overlook Crater. J. Volcanol. Geotherm. Res. 300, 81–94. https://doi.org/10.1016/j.jvolgeores.2014.12.004

Kern, C., Werner, C., Elias, T., Sutton, A.J., Lübcke, P., 2013. Applying UV cameras for SO2 detection to distant or optically thick volcanic plumes. J. Volcanol. Geotherm. Res. 262, 80–89. https://doi.org/10.1016/j.jvolgeores.2013.06.009

Klein, A., Lübcke, P., Bobrowski, N., Kuhn, J., Platt, U., 2017. Plume propagation direction determination with SO 2 cameras. Atmos. Meas. Tech 10, 979–987. https://doi.org/10.5194/amt-10-979-2017

Kremers, S., Wassermann, J., Meier, K., Pelties, C., van Driel, M., Vasseur, J., Hort, M., 2013. Inverting the source mechanism of Strombolian explosions at Mt. Yasur, Vanuatu, using a multi-parameter dataset. J. Volcanol. Geotherm. Res. 262, 104–122. https://doi.org/10.1016/j.jvolgeores.2013.06.007

Laiolo, M., Massimetti, F., Cigolini, C., Ripepe, M., Coppola, D., 2018. Long-term eruptive trends from space-based thermal and SO2 emissions: a comparative analysis of Stromboli, Batu Tara and Tinakula volcanoes. Bull. Volcanol. 80, 1–19. https://doi.org/10.1007/s00445-018-1242-0

Liu, E.J., Wood, K., Mason, E., Edmonds, M., Aiuppa, A., Giudice, G., Bitetto, M., Francofonte, V., Burrow, S., Richardson, T., Watson, M., Pering, T.D., Wilkes, T.C., McGonigle, A.J.S., Velasquez, G., Melgarejo, C., Bucarey, C., 2019. Dynamics of Outgassing and Plume Transport Revealed by Proximal Unmanned Aerial System (UAS) Measurements at Volcán Villarrica, Chile. Geochemistry, Geophys. Geosystems 20, 730–750. https://doi.org/10.1029/2018GC007692

Lübcke, P., Bobrowski, N., Illing, S., Kern, C., Alvarez Nieves, J.M., Vogel, L., Zielcke, J., Delgado Granados, H., Platt, U., 2013. On the absolute calibration of SO_2 cameras. Atmos. Meas. Tech. 6, 677–696. https://doi.org/10.5194/amt-6-677-2013

Marchetti, E., Ripepe, M., Harris, A.J.L., Delle Donne, D., 2009. Tracing the differences between Vulcanian and Strombolian explosions using infrasonic and thermal radiation energy. Earth Planet. Sci. Lett. 279, 273–281. https://doi.org/10.1016/j.epsl.2009.01.004

McCormick, B.T., Herzog, M., Yang, J., Edmonds, M., Mather, T.A., Carn, S.A., Hidalgo, S., Langmann, B., 2014. A comparison of satellite- and ground-based measurements of SO2 emissions from tungurahua volcano, Ecuador. J. Geophys. Res. 119, 4264–4285. https://doi.org/10.1002/2013JD019771

McGonigle, A.J.S., Aiuppa, A., Ripepe, M., Kantzas, E.P., Tamburello, G., 2009. Spectroscopic capture of 1 Hz volcanic SO2 fluxes and integration with volcano geophysical data. Geophys. Res. Lett. 36, 1–5. https://doi.org/10.1029/2009GL040494

McGonigle, A.J.S., Hilton, D.R., Fischer, T.P., Oppenheimer, C., 2005. Plume velocity determination for volcanic SO2 flux measurements. Geophys. Res. Lett. 32, 1–4. https://doi.org/10.1029/2005GL022470

McGonigle, A.J.S., Pering, T.D., Wilkes, T.C., Tamburello, G., D'Aleo, R., Bitetto, M., Aiuppa, A., Willmott, J.R., 2017. Ultraviolet Imaging of Volcanic Plumes: A New Paradigm in Volcanology. Geosciences 7, 68. https://doi.org/10.3390/geosciences7030068

Meier, K., Hort, M., Wassermann, J., Garaebiti, E., 2016. Strombolian surface activity regimes at Yasur volcano, Vanuatu, as observed by Doppler radar, infrared camera and infrasound. J. Volcanol. Geotherm. Res. 322, 184–195. https://doi.org/10.1016/j.jvolgeores.2015.07.038

Métrich, N., Allard, P., Aiuppa, A., Bani, P., Bertagnini, A., Shinohara, H., Parello, F., Di Muro, A., Garaebiti, E., Belhadj, O., Massare, D., 2011. Magma and Volatile Supply to Post-collapse Volcanism and Block Resurgence in Siwi Caldera (Tanna Island, Vanuatu Arc). J. Petrol. 52, 1077–1105. https://doi.org/10.1093/petrology/egr019

Mori, T., Burton, M., 2009. Quantification of the gas mass emitted during single explosions on Stromboli with the SO2 imaging camera. J. Volcanol. Geotherm. Res. 188, 395–400. https://doi.org/10.1016/j.jvolgeores.2009.10.005

Mori, T., Burton, M., 2006. The SO_2 camera: A simple, fast and cheap method for ground-based imaging of SO_2 in volcanic plumes. Geophys. Res. Lett. 33, L24804. https://doi.org/10.1029/2006GL027916

Oppenheimer, C., Bani, P., Calkins, J.A., Burton, M.R., Sawyer, G.M., 2006. Rapid FTIR sensing of volcanic gases released by Strombolian explosions at Yasur volcano, Vanuatu. Appl. Phys. B 85, 453–460. https://doi.org/10.1007/s00340-006-2353-4

Oppenheimer, C., Lomakina, A.S., Kyle, P.R., Kingsbury, N.G., Boichu, M., 2009. Pulsatory magma supply to a phonolite lava lake. Earth Planet. Sci. Lett. 284, 392–398. https://doi.org/10.1016/j.epsl.2009.04.043

Parfitt, E.A., 2004. A discussion of the mechanisms of explosive basaltic eruptions. J. Volcanol. Geotherm. Res. 134, 77–107. https://doi.org/10.1016/j.jvolgeores.2004.01.002

Patrick, M.R., Harris, A.J.L., Ripepe, M., Dehn, J., Rothery, D.A., Calvari, S., 2007. Strombolian explosive styles and source conditions: Insights from thermal (FLIR) video.

Bull. Volcanol. 69, 769–784. https://doi.org/10.1007/s00445-006-0107-0
Pering, T.D., Ilanko, T., Liu, E.J., 2019a. Periodicity in Volcanic Gas Plumes: A Review and Analysis. Geosci. 2019, Vol. 9, Page 394 9, 394. https://doi.org/10.3390/GEOSCIENCES9090394
Pering, T.D., Ilanko, T., Wilkes, T.C., England, R.A., Silcock, S.R., Stanger, L.R., Willmott, J.R., Bryant, R.G., McGonigle, A.J.S., 2019b. A Rapidly Convecting Lava Lake at Masaya Volcano, Nicaragua. Front. Earth Sci. 6, 241. https://doi.org/10.3389/feart.2018.00241
Pering, T.D., McGonigle, A.J.S., 2018. Combining Spherical-Cap and Taylor Bubble Fluid Dynamics with Plume Measurements to Characterize Basaltic Degassing. Geosciences 8, 42. https://doi.org/10.3390/geosciences8020042
Pering, T.D., McGonigle, A.J.S., James, M.R., Capponi, A., Lane, S.J., Tamburello, G., Aiuppa, A., 2017. The dynamics of slug trains in volcanic conduits: Evidence for expansion driven slug coalescence. J. Volcanol. Geotherm. Res. 348, 26–35. https://doi.org/10.1016/J.JVOLGEORES.2017.10.009
Pering, T.D., McGonigle, A.J.S., James, M.R., Tamburello, G., Aiuppa, A., Delle Donne, D., Ripepe, M., 2016. Conduit dynamics and post-explosion degassing on Stromboli: a combined UV camera and numerical modelling treatment. Geophys. Res. Lett. https://doi.org/10.1002/2016GL069001
Pering, T. D., McGonigle, A.J.S., James, M.R., Tamburello, G., Aiuppa, A., Delle Donne, D., Ripepe, M., 2016. Conduit dynamics and post explosion degassing on Stromboli: A combined UV camera and numerical modeling treatment. Geophys. Res. Lett. 43, 5009–5016. https://doi.org/10.1002/2016GL069001
Pering, T.D., Tamburello, G., McGonigle, A.J.S., Aiuppa, A., Cannata, A., Giudice, G., Patanè, D., 2014. High time resolution fluctuations in volcanic carbon dioxide degassing from Mount Etna. J. Volcanol. Geotherm. Res. 270, 115–121. https://doi.org/10.1016/j.jvolgeores.2013.11.014
Pering, T.D., Tamburello, G., McGonigle, A.J.S., Aiuppa, A., James, M.R., Lane, S.J., Sciotto, M., Cannata, A., Patanè, D., 2015. Dynamics of mild strombolian activity on Mt. Etna. J. Volcanol. Geotherm. Res. 300, 103–111. https://doi.org/10.1016/j.jvolgeores.2014.12.013
Peters, N., Hoffmann, A., Barnie, T., Herzog, M., Oppenheimer, C., 2015. Use of motion estimation algorithms for improved flux measurements using SO2 cameras. J. Volcanol. Geotherm. Res. 300, 58–69. https://doi.org/10.1016/j.jvolgeores.2014.08.031
Peters, N., Oppenheimer, C., 2018. Plumetrack: Flux calculation software for UV cameras. Comput. Geosci. 118, 86–90. https://doi.org/10.1016/j.cageo.2018.05.014
Platt, U., Lübcke, P., Kuhn, J., Bobrowski, N., Prata, F., Burton, M., Kern, C., 2015. Quantitative imaging of volcanic plumes — Results, needs, and future trends. J. Volcanol. Geotherm. Res. 300, 7–21. https://doi.org/10.1016/j.jvolgeores.2014.10.006
Polacci, M., Baker, D.R.D., La Rue, Alexandra, Mancini, L., Allard, P., Rue, A La, Mancini, L., 2012. Degassing behaviour of vesiculated basaltic magmas: an example from Ambrym volcano, Vanuatu Arc 233–234, 55–64. https://doi.org/10.1016/J.JVOLGEORES.2012.04.019
Ripepe, M., Harris, A.J.L., Carniel, R., 2002. Thermal, seismic and infrasonic evidences of variable degassing rates at Stromboli volcano. J. Volcanol. Geotherm. Res. 118, 285–297. https://doi.org/10.1016/S0377-0273(02)00298-6
Ripepe, M., Harris, A.J.L., Marchetti, E., 2005. Coupled thermal oscillations in explosive activity at different craters of Stromboli volcano. Geophys. Res. Lett. 32, 1–4. https://doi.org/10.1029/2005GL022711
Ripepe, M., Marchetti, E., 2002. Array tracking of infrasonic sources at Stromboli volcano.

Geophys. Res. Lett. 29, 33-1-33–4. https://doi.org/10.1029/2002gl015452
Salvatore, V., Silleni, A., Corneli, D., Taddeucci, J., Palladino, D.M., Sottili, G., Bernini, D., Andronico, D., Cristaldi, A., 2018. Parameterizing multi-vent activity at Stromboli Volcano (Aeolian Islands, Italy). Bull. Volcanol. 80, 64. https://doi.org/10.1007/s00445-018-1239-8
Seyfried, R., Freundt, A., 2000. Experiments on conduit flow and eruption behavior of basaltic volcanic eruptions. J. Geophys. Res. 105, 23727. https://doi.org/10.1029/2000JB900096
Shinohara, H., Ohminato, T., Takeo, M., Tsuji, H., 2015. Monitoring of volcanic gas composition at Asama volcano, Japan, during 2004–2014. J. Volcanol.
Shinohara, H., Witter, J.B., 2005. Volcanic gases emitted during mild Strombolian activity of Villarrica volcano, Chile. Geophys. Res. Lett. 32, L20308. https://doi.org/10.1029/2005GL024131
Simons, B.C., Jolly, A.D., Eccles, J.D., Cronin, S.J., 2020. Spatiotemporal Relationships between Two Closely-spaced Strombolian-style Vents, Yasur, Vanuatu. Geophys. Res. Lett. 47. https://doi.org/10.1029/2019GL085687
Spina, L., Taddeucci, J., Cannata, A., Gresta, S., Lodato, L., Privitera, E., Scarlato, P., Gaeta, M., Gaudin, D., Palladino, D.M., 2016. "Explosive volcanic activity at Mt. Yasur: A characterization of the acoustic events (9–12th July 2011)." J. Volcanol. Geotherm. Res. 322, 175–183. https://doi.org/10.1016/j.jvolgeores.2015.07.027
Spina, A. La, Burton, M.R., Harig, R., Mure, F., Rusch, P., Jordan, M., Caltabiano, T., 2013. New insights into volcanic processes at Stromboli from Cerberus , a remote-controlled open-path FTIR scanner system. J. Volcanol. Geotherm. Res. 249, 66–76. https://doi.org/10.1016/j.jvolgeores.2012.09.004
Suckale, J., Keller, T., Cashman, K. V, Persson, P.-O., 2016. Flow-to-fracture transition in a volcanic mush plug may govern normal eruptions at Stromboli. Geophys. Res. Lett. 43, 12071–12081. https://doi.org/10.1002/2016GL071501
Sweeney, D., Kyle, P.R., Oppenheimer, C., 2008. Sulfur dioxide emissions and degassing behavior of Erebus volcano, Antarctica. J. Volcanol. Geotherm. Res. 177, 725–733. https://doi.org/10.1016/j.jvolgeores.2008.01.024
Szramek, L., Gardner, J.E., Larsen, J., 2006. Degassing and microlite crystallization of basaltic andesite magma erupting at Arenal Volcano, Costa Rica. J. Volcanol. Geotherm. Res. 157, 182–201. https://doi.org/10.1016/j.jvolgeores.2006.03.039
Taddeucci, J., Edmonds, M., Houghton, B., James, M.R., Vergniolle, S., 2015. Hawaiian and Strombolian Eruptions, in: The Encyclopedia of Volcanoes. Elsevier, pp. 485–503. https://doi.org/10.1016/b978-0-12-385938-9.00027-4
Taddeucci, J., Scarlato, P., Capponi, A., Del Bello, E., Cimarelli, C., Palladino, D.M., Kueppers, U., Bello, E. Del, Cimarelli, C., Palladino, D.M., Kueppers, U., 2012. High-speed imaging of Strombolian explosions: The ejection velocity of pyroclasts. Geophys. Res. Lett. 39, 1–6. https://doi.org/10.1029/2011GL050404
Tamburello, G., Aiuppa, A., Kantzas, E.P., Mcgonigle, A.J.. S., Ripepe, M., 2012. Passive vs . active degassing modes at an open-vent volcano (Stromboli , Italy). Earth Planet. Sci. Lett. 359–360, 106–116. https://doi.org/10.1016/j.epsl.2012.09.050
Tamburello, G., Aiuppa, A., McGonigle, A.J.S., Allard, P., Cannata, A., Giudice, G., Kantzas, E.P., Pering, T.D., 2013. Periodic volcanic degassing behavior: The Mount Etna example. Geophys. Res. Lett. 40, 4818–4822. https://doi.org/10.1002/grl.50924
Thielicke, W., 2014. The flapping flight of birds : analysis and application. [S.n.].
Thielicke, W., Stamhuis, E.J., 2014. PIVlab – Towards User-friendly, Affordable and Accurate Digital Particle Image Velocimetry in MATLAB. J. Open Res. Softw. 2. https://doi.org/10.5334/jors.bl

Vergniolle, S., Boichu, M., Caplan-Auerbach, J., 2004. Acoustic measurements of the 1999 basaltic eruption of Shishaldin volcano, Alaska 1. Origin of Strombolian activity. J. Volcanol. Geotherm. Res. 137, 109–134. https://doi.org/10.1016/j.jvolgeores.2004.05.003

Vergniolle, S., Jaupart, C., 1986. Separated two-phase flow and basaltic eruptions. J. Geophys. Res. Solid Earth 91, 12842–12860. https://doi.org/10.1029/JB091iB12p12842

Wilkes, T., McGonigle, A., Pering, T., Taggart, A., White, B., Bryant, R., Willmott, J., Wilkes, T.C., McGonigle, A.J.S., Pering, T.D., Taggart, A.J., White, B.S., Bryant, R.G., Willmott, J.R., 2016. Ultraviolet Imaging with Low Cost Smartphone Sensors: Development and Application of a Raspberry Pi-Based UV Camera. Sensors 16, 1649. https://doi.org/10.3390/s16101649

Wilkes, T., Pering, T., McGonigle, A., Tamburello, G., Willmott, J., Wilkes, T.C., Pering, T.D., McGonigle, A.J.S., Tamburello, G., Willmott, J.R., 2017. A Low-Cost Smartphone Sensor-Based UV Camera for Volcanic SO2 Emission Measurements. Remote Sens. 9, 27. https://doi.org/10.3390/rs9010027

Williams-Jones, G., Horton, K.A., Elias, T., Garbeil, H., Mouginis-Mark, P.J., Sutton, A.J., Harris, A.J.L., 2006. Accurately measuring volcanic plume velocity with multiple UV spectrometers. Bull. Volcanol. 68, 328–332. https://doi.org/10.1007/s00445-005-0013-x

Woitischek, J., Woods, A.W., Edmonds, M., Oppenheimer, C., Aiuppa, A., Pering, T.D., Ilanko, T., D'Aleo, R., Garaebiti, E., n.d. Strombolian eruptions and dynamics of magma degassing at Yasur Volcano (Vanuatu). J. Volcanol. Geotherm. Res.